Structural design of composite materials with superior mechanical behaviors: lesson from the microstructure of nacre and enamel

Hanfeng Zhai

Department of Mechanics,
School of Mechanics and Engineering Science,
Shanghai University

June 22, 2020

CAD Application in Structural Mechanics

Structural design of composite materials with superior mechanical behaviors: lesson from the microstructure of nacre and enamel

Abstract

Biomaterials like nacre and tooth enamel display spectacular mechanical properties such as high stiffness, high strength, high toughness, and fracture durability. Such properties are exhibited by their natural developed structures, both employ common characteristics: consisting of hard mineral inclusions and soft protein matrix. Here, we build models, representative, for nacre, and enamel consisting of hard inclusions and soft matrix, respectively. We give the soft matrix a plastic property based on their natural mechanics. We thence calculate the 1 and 2-directional stiffness of the two structures and present their von Mises' stress, directional stress, and directional strain distribution, respectively. For what is more, we estimate the fracture resistance of the two structures based on the assumption that the failure occurs on the soft matrix in which the shear stress reaches a critical value. We hence deduce that the nacre displays better 1-directional stiffness and enamel displays better 2-directional stiffness. The shear stress-displacement diagrams in each direction are also presented indicating the nacre is more likely to fail in 1-direction and enamel is more likely in 2-direction. Based on the results we present an optimized model taking the characters from both the nacre and enamel. Results show that the optimized model exhibits higher stiffness in both the two directions and evidently better crack resistance in 2-direction.

Keywords: stiffness; fracture; biomaterials; biomechanics; bioinspired structure

Introduction

There are many species in nature. These creatures have evolved to obtain materials with superior mechanical properties with regard to their natural environment, which are called biomaterials. Biomaterials is among the key issue in structural design due to its spectacular performance. Human dentin is one of them. Dentin displays high crack resistance and hardening yielding behavior ([1], [3], [4]). Also, cortical bone displays similar crack resistance property ([2], [6], [7], [8]). The constitutive models for dentin and cortical bone are similar to many aspects, with hardening plastic property that exhibits superior fracture resistance ([1], [6]). Also, biomaterials composites all display similar hierarchical structure, which could be depicted by "architectured", in which hard inclusions bonded with soft matrix ([5], [7]). Mirkhalafa *et al.* [5] employ the CAD approach to estimate the hierarchical structure of enamel and nacre, which is the key essence studied in this paper.

As mentioned, the microstructure of nacre displays high durability, stiffness, and crack resistance, which could be illustrated as the "Brick-and-Mortar" structure. Such a structure is well studied by scholars. An experimental approach employing the three-point bending method the tests the BM structure's fracture resistance and present the crack propagation law illustrated by testing [9]. Experimental approaches illustrated the fracture mechanism of nacre and properties is explained by mesoscopic models [10]. For what is more, the tensile stiffness and strength, and fracture resistance are studied and tested by carrying out experiment directly studying the nacre's mechanical properties [11]. A numerical approach to study its bending

properties by studying the layer numbers effect on the nacre's total bending load fracture resistance presents a complex relationship between the layer numbers and its mechanical properties [12]. Plus, spatial orientation and arrangement of such a structure are studied by the experimental approach [13].

Enamel is the hardest and most highly mineralized tissue of mammalian teeth, which displays high fracture resistance and complex hierarchical architecture structure [14]. Furthermore, the enamel section displays different architecture in certain areas, and the crack propagated along with the protein within rods [15]. Such a character is estimated and studied through an experimental approach revealing how the decussation structure resists crack growth with regards to directions and regions ([15], [16]). Not only humans, mammals such as wild wolf's teeth also exhibit high toughness and durability with a hierarchical structure, consisting of hard rods and soft protein matrix [17]. The microscopic structure of the mentioned "rod" is hence estimated through decent experiments and inspire a new structural design [18], whose thought trace is similarly employed in this paper.

Method

Problem Formulation

As mentioned in the preceding chapter, for both the nacre and the enamel's microstructure displays high stiffness and durability, which is highly focused in this paper. Their structural arrangement is the key issue studied. Hence, the modeling part is significantly important to ensure the main character is described properly with consideration of a universal application for the whole structure.

Initially, the modelling for the nacre structural design is shown in Figure 1(c), which is also described by the "Brick-and-Mortar" structure. With consideration of the chemical components, the hard inclusion usually consists of minerals, and the soft matrix consists of organic protein.

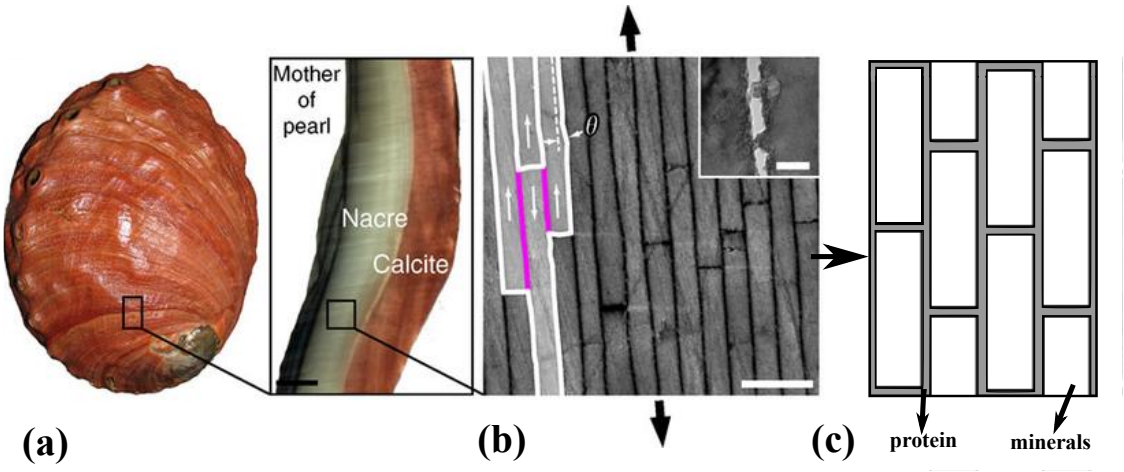

Fig. 1 The structural illustration of nacre. (a) photo of the nacre. (b) SEM photo of the nacre's microscopic structure. (c) schematic illustration of the nacre microscopic structure's modelling.

The modelling for the nacre structural design is shown as in Figure 2(c), in which the oval part is the enamel rod consisting of minerals surrounded by soft protein.

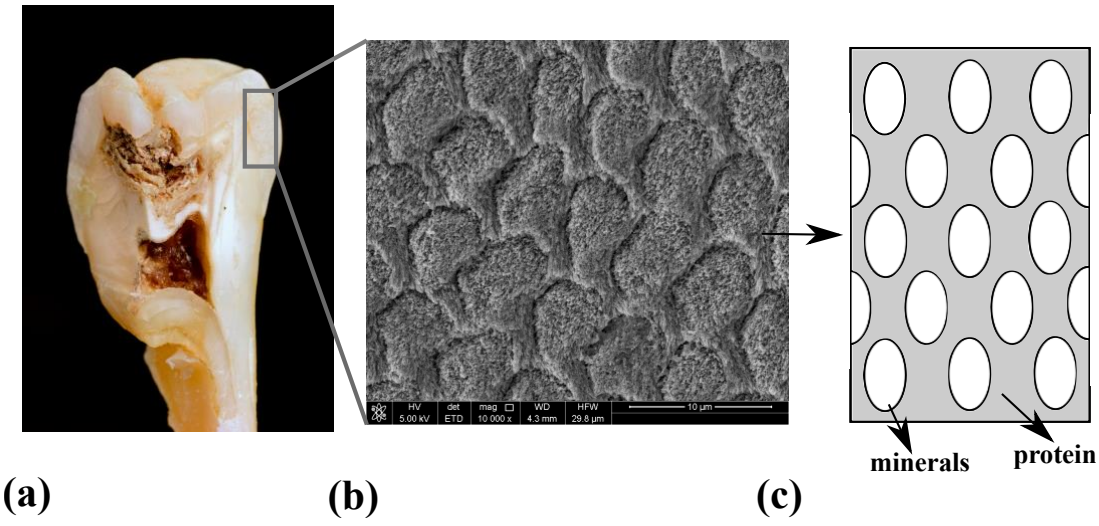

Fig. 2 The structural illustration of tooth enamel. (a) photo of the human tooth. (b) SEM photo of the enamel's microscopic structure. (c) schematic illustration of the enamel microscopic structure's modelling.

From both the scanning electron microscope (SEM) picture taken at a microscopic level of nacre and enamel shown in Figure 1(b) and Figure 2(b), we build the given model trying the illustrate the basic characters of the structure with a wide representation for the whole material. For what is more, the mechanical parameters for these materials are shown as in Table 1, in which the soft protein matrix employs a plastic property, as illustrated by An. *et al* ([1], [2], [3], [4]) and Ghazlana. *et al* [12]. We employ a perfect plastic model for the soft matrix. Admittedly, hard mineral inclusion displays plastic properties too [1], yet based on the previous analyzation of biomaterials' fracture, crack does not usually propagate on hard minerals and mostly the minerals have not reached the yield stress when the composite fails ([5], [9], [12], [15], [16], [18]), hence the plastic property of hard inclusion is not considered in the study.

Material	Elastic Modulus	Poisson's Ratio	Yield Stress
Mineral	20.7GPa	0.3	
Protein	1MPa	0.3	9MPa

Tab. 1 Mechanical parameters of the mineral and protein carried out for simulation.

Stiffness Calculation

To estimate the stiffness on each direction of the presented biomaterials, the elastic moduli for enamel and nacre are to be calculated with the set parameters. To delineate such, the mean strain is calculated taking the form

$$\begin{cases} \overline{\varepsilon_x} = \dfrac{u_x}{a} \\ \overline{\varepsilon_y} = \dfrac{u_y}{b} \end{cases} \tag{1}$$

In which u_x and u_y are displacements in 1 and 2 directions, respectively; a and b are length and width of the presented models, respectively.

The mean stress takes the form:

$$\begin{cases} \overline{\sigma_x} = \sum_{y=0}^{b} \frac{R_x(a,y)}{b} \\ \overline{\sigma_y} = \sum_{x=0}^{a} \frac{R_y(x,b)}{a} \end{cases} \tag{2}$$

In which R_x and R_y are reactional forces in 1 and 2 directions, respectively.

The 1 and 2-directional elastic moduli of the composite can thence be calculated through Equation 1 and 2:

$$\begin{cases} E_x = \frac{\overline{\sigma_x}}{\overline{\varepsilon_x}} \\ E_y = \frac{\overline{\sigma_y}}{\overline{\varepsilon_y}} \end{cases} \tag{3}$$

Fracture Estimation

As mentioned and presented through both numerical and experimental methods, the fracture and failure of the bioinspired structural materials occurs at the soft protein matrix and propagated along with such material in the whole structure ([5], [9], [12], [15], [16], [18]). For what is more, such local failure usually exhibits plastic properties that might resist the crack growth ([1], [2], [3], [4], [12]). Hence, here, we adopted two basic hypotheses for the composites' failure in simulation: 1). The failure occurs on matrix when shear stress reaches a specific critical value. 2). The matrix displays plastic properties in the fracture process. Usually, the displacement loaded can be directly measured. Therefore, we present the relation between the matrix shear stress with the composites' loading displacement to estimate and study the fracture properties.

Results and Discussion

Stiffness Calculation

Based on the model, the mechanical distribution can hence be calculated for the structures as given. The von Mises stress, 1-directional stress and 1-directional strain distribution of the enamel undergoing 1-directional loading are shown as in Figure 3.

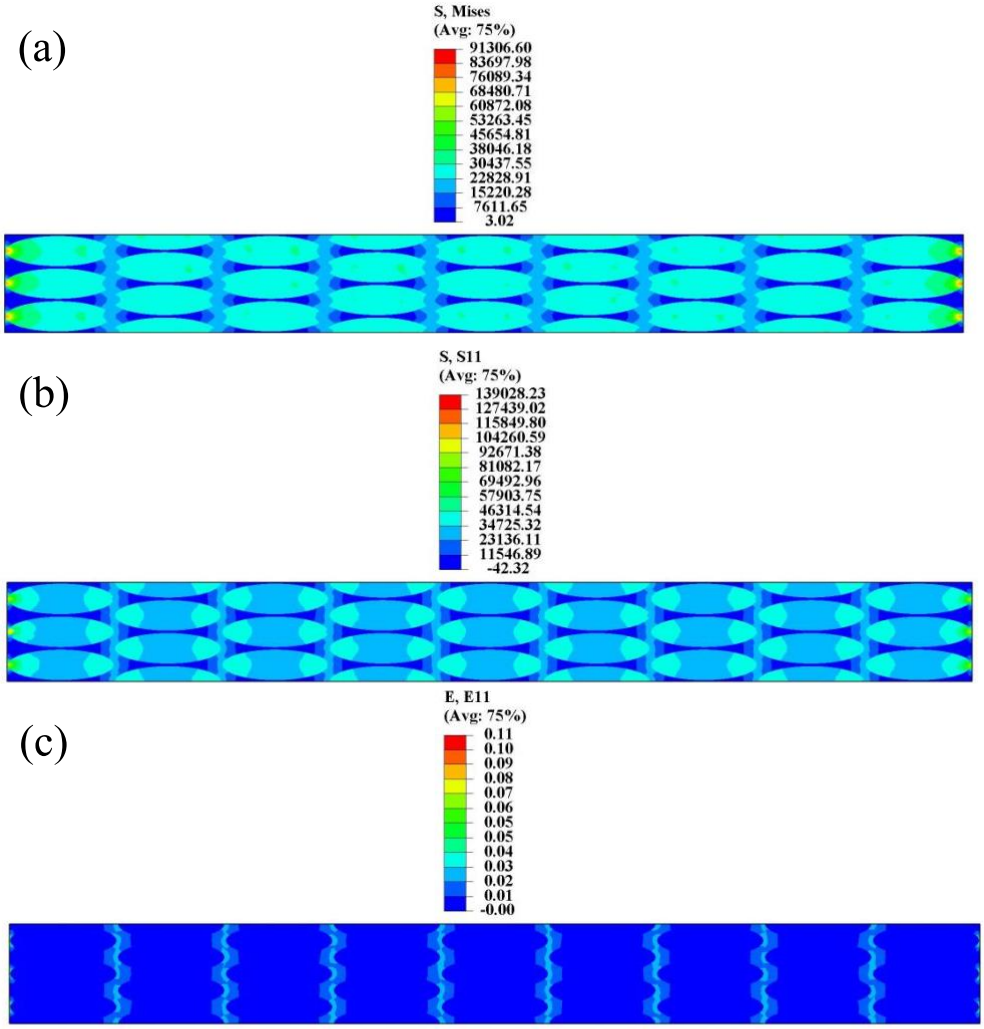

Fig. 3 The enamel's 1-directional mechanical distribution carried out for uniaxial tensile loading. (a) von Mises stress distribution. (b) 1-directional stress distribution. (c) 1-directional strain distribution.

From Figure 3(a) and Figure 3(b) one can discern the hard inclusion takes higher stress value due to its high stiffness, especially, the 1-directional stress is unevenly

distributed on the hard inclusions as shown in Figure 3(b). As shown in Figure 3(c) one deduces that the contact surface undergoes higher strain values, which might also indicate local failure or deformation.

Similarly, the von Mises stress, 1-directional stress, and 1-directional strain distribution of the enamel undergoing 2-directional loading are shown as in Figure 4.

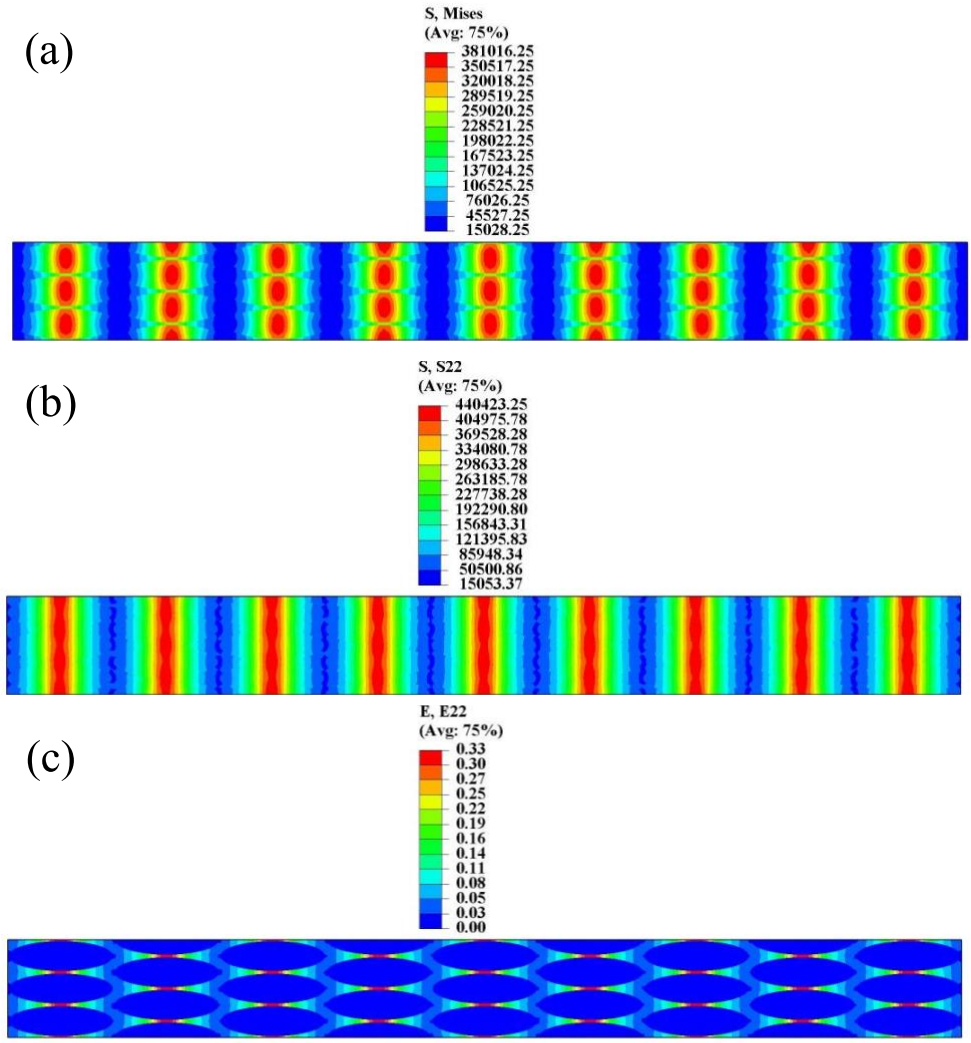

Fig. 4 The enamel's 2-directional mechanical distribution carried out for uniaxial tensile loading. (a) von Mises stress distribution. (b) 2-directional stress distribution. (c) 1-directional strain distribution.

Comparing Figure 4(a) with Figure 4(b) one could discern that the 1-directional stress also makes a robust effect on the Mises stress distribution due to the variance

occurs on the rods' contact edge. From Figure 4(c) one could observe strain concentration on inclusion-matrix contact edge.

For the nacre structure, the von Mises stress, 1-directional stress and 1-directional strain distribution undergoing 1-directional loading are shown as in Figure 5.

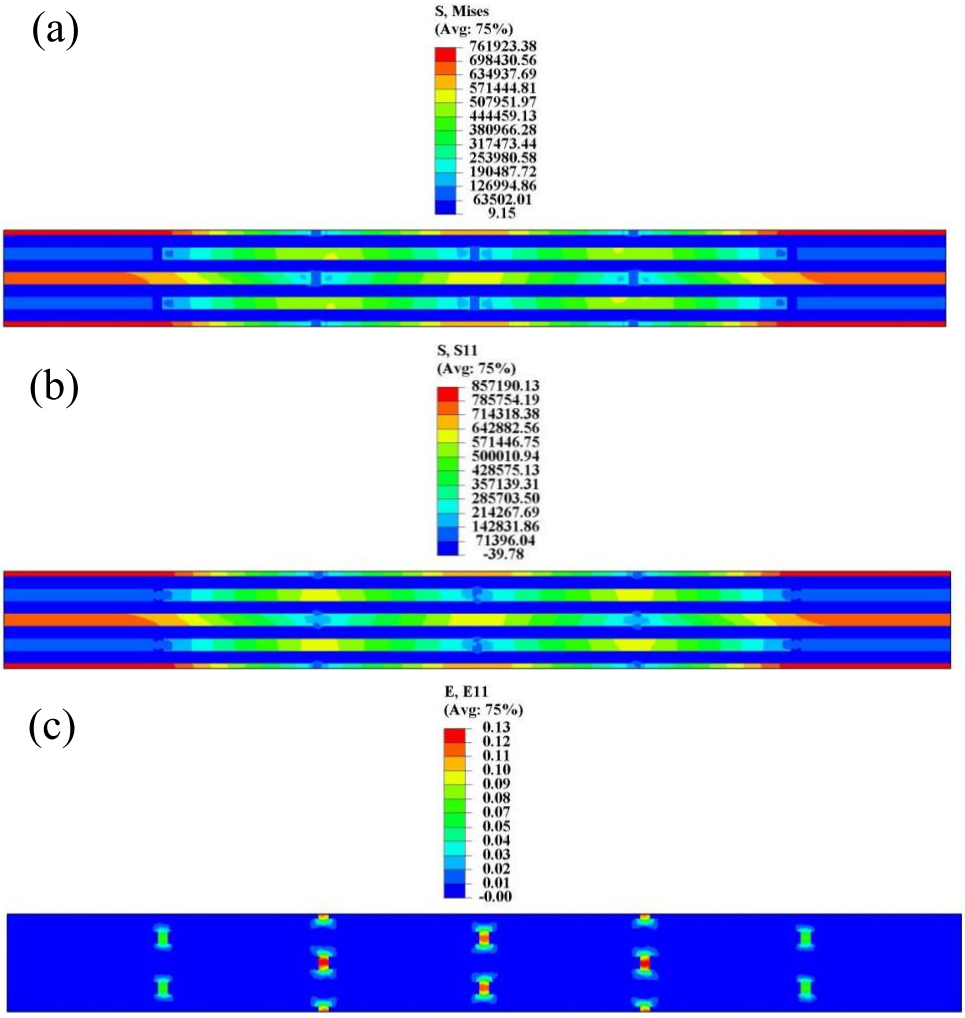

Fig. 5 The nacre's 1-directional mechanical distribution carried out for uniaxial tensile loading. (a) von Mises stress distribution. (b) 1-directional stress distribution. (c) 1-directional strain distribution.

From Figure 5 one could observe that the nacre's 2-directional stress makes little influence on the whole structure's stress distribution comparing Figure 5(a) and Figure 5(b). A strain concentration occurs at the soft matrix between contacts of nacre

inclusion as shown in Figure 5(c). Such a concentration indicates a possible dislocation between inclusion layers.

The von Mises stress, 2-directional stress and 2-directional strain distribution of the nacre structure undergoing 2-directional loading are shown as in Figure 6.

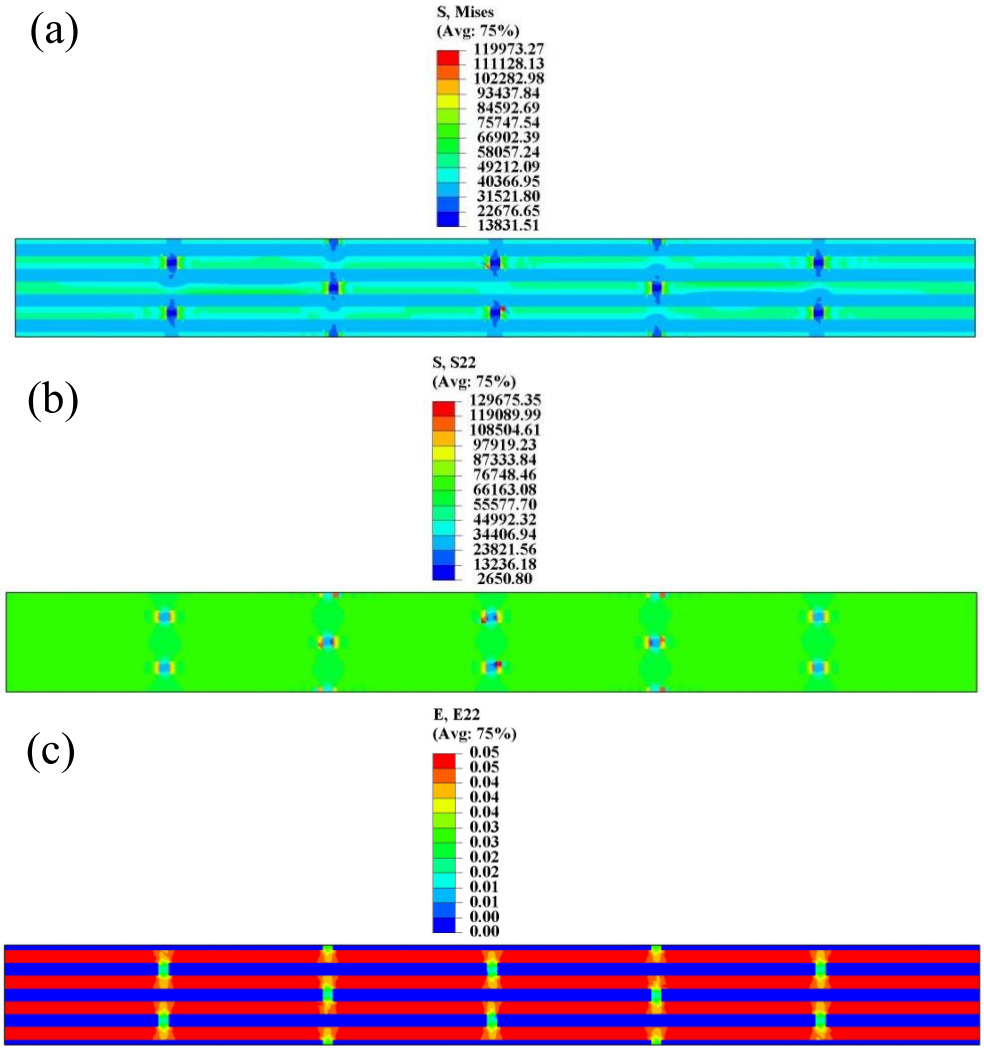

Fig. 6 The nacre's 2-directional mechanical distribution carried out for uniaxial tensile loading. (a) von Mises stress distribution. (b) 2-directional stress distribution. (c) 2-directional strain distribution.

Comparing Figure 6(a) with Figure 6(b) one observe that the nacre's 2-directional stress does not play the key role in the total stress distribution. Figure 6(c) shows that strain concentrates on hard inclusions undergoes 2-directional loading.

As illustrated in Figure 2-Figure 6, one could deduce a basic stiffness for each direction of each composite materials based on the stress-strain distribution. Applied with Equation 1-Equation 3 one could calculate the stiffness of each material as given in Figure 7.

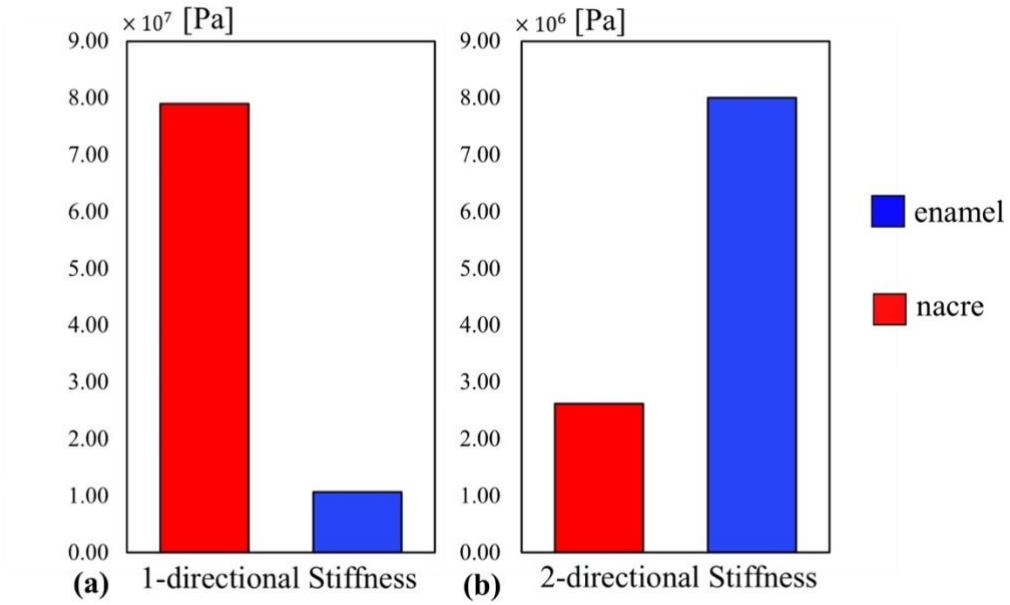

Fig. 7 The nacre and enamel structured composites' 1 and 2-directional stiffness.

As shown in Figure 7 the nacre's 1-directional stiffness is much higher than what is for enamel, yet the enamel's 2-directional stiffness is much higher than nacre. Firstly, the longitudinal lengthy hard inclusion in nacre could provide support for its longitudinal stiffness. Yet, for the higher value of the 2-directional stiffness of enamel, the circular shape and the evenly distributed contact area of the hard inclusion and the cross arranged rods could be a possible explanation.

Hence, we can adopt a basic thought trace that if a structural design contains characteristics of enamel and nacre in both the two directions might exhibit higher stiffness in both the two directions.

Fracture Estimation

As illustrated in the last chapter, the matrix (protein) fails when shear stress reaches a critical value. Thence, the shear stress distribution of enamel protein is given as shown in Figure 8(a) and the 1-directional displacement distribution when a 1-direction loading is applied is shown in Figure 8(b).

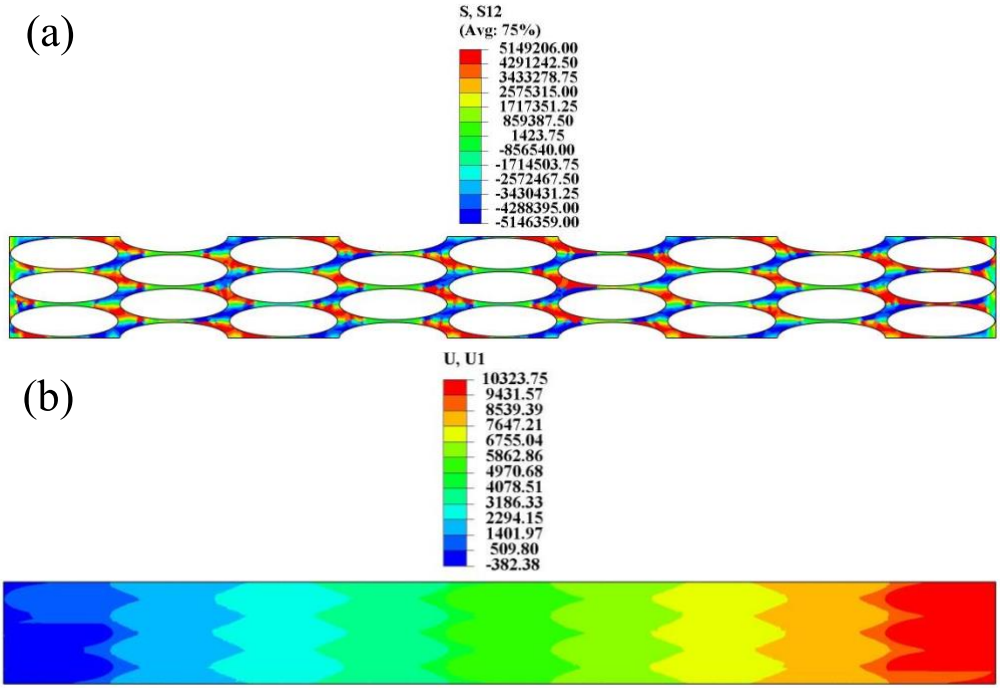

Fig. 8 The enamel's 1-directional mechanical distribution carried out for uniaxial tensile loading. (a) shear stress distribution. (b) 1-directional displacement distribution.

From Figure 8(a) one observes that there is a high concentration of shear stress occurs along with the 1-directional enamel rod's contact, which might indicate a possible protein fracture mechanism. For what is more, the high concentration of stress value is parallel with the 1-direction, implying an indicator of the mechanism to prevent the fracture take place along the axis perpendicular to the loading direction.

Figure 9 presents the shear stress distribution of enamel protein and the 2-directional displacement distribution when a 2-direction loading is applied.

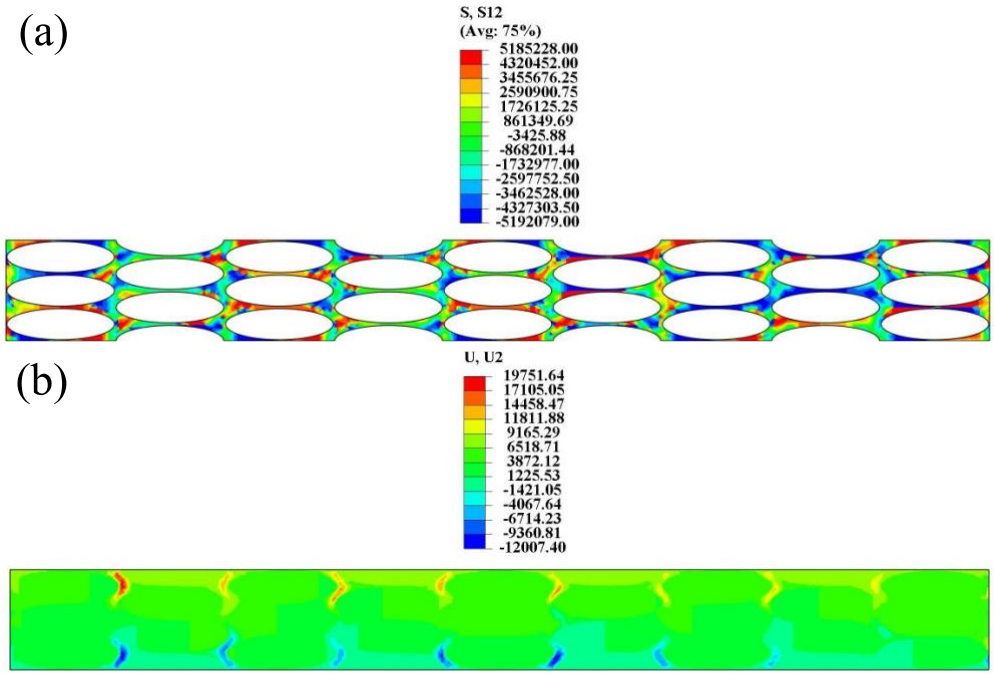

Fig. 9 The enamel's 2-directional mechanical distribution carried out for uniaxial tensile loading. (a) shear stress distribution. (b) 2-directional displacement distribution.

From what is shown in Figure 9(a), a strain concentration occurs on the enamel rods' 2-directional contact edge. Howbeit, similar strain distribution pattern as discussed in Figure 8(a) that shear stress concentration does not occur along edges perpendicular to the loading edge indicates a mechanism that can effectively resist fracture and crack propagation. From Figure 9(b) as the loading displacement gives there are deformation occurs along the inclusion's 1-directional edges. Such phenomena contend a possible local malposition occurs that might lead to sliding of the enamel rod and its surrounding organic protein.

Figure 10 presents the shear stress distribution of nacre protein and the 1-directional displacement distribution when a 1-direction loading is applied. Figure 11 presents the shear stress distribution of nacre protein and the 2-directional displacement distribution when a 2-direction loading is applied.

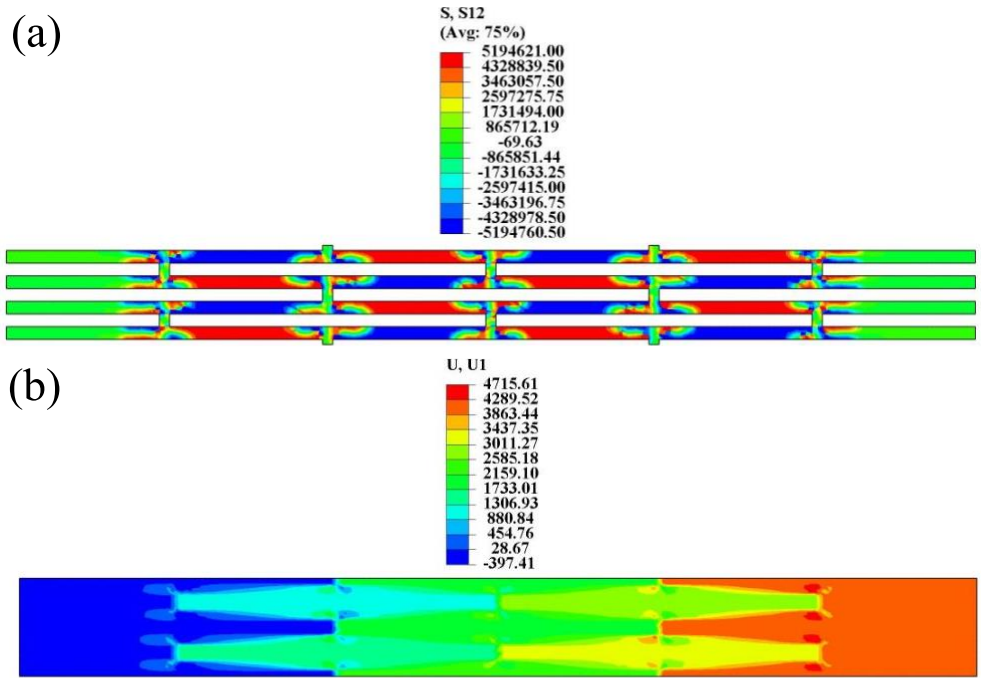

Fig. 10 The nacre's 1-directional mechanical distribution carried out for uniaxial tensile loading. (a) shear stress distribution. (b) 1-directional displacement distribution.

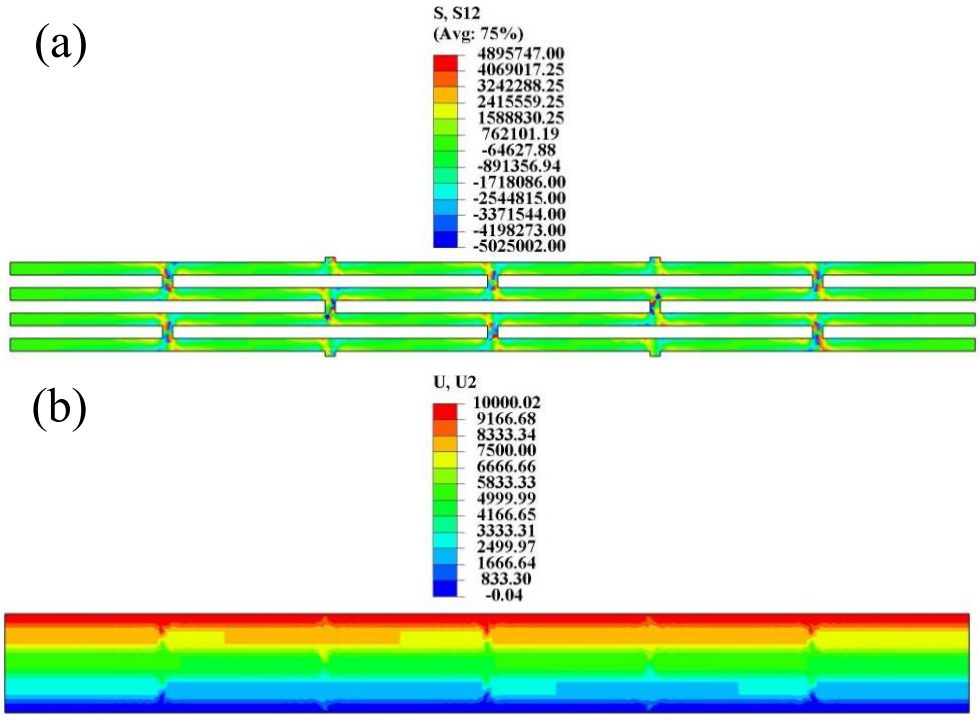

Fig. 11 The nacre's 2-directional mechanical distribution carried out for uniaxial tensile loading. (a) shear stress distribution. (b) 2-directional displacement distribution.

Similarly, as it is presented in Figure 10, one observes that a shear stress concentration occurs along the matrix longitudinal axis, but no concentration along the axis perpendicular to the loading direction, also indicating a fracture prevention mechanism. But the nacre's 2-directional loading shows a shear stress concentration perpendicular with the loading direction, contending a higher possibility for local failure. But the bonding hard inclusions could provide a robust cohesion to increase the local strength.

As it is mentioned in the preceding chapter, we adopt a perfectly plastic model for the matrix as investigating its possibility of local failure. Due to the displacement that can be directly measured by modern equipment, we present shear stress-displacement curves as guidelines for judgment of the local failure.

Here, Figure 12 presents the shear stress-displacement of the 1-directional loading of enamel and nacre, respectively.

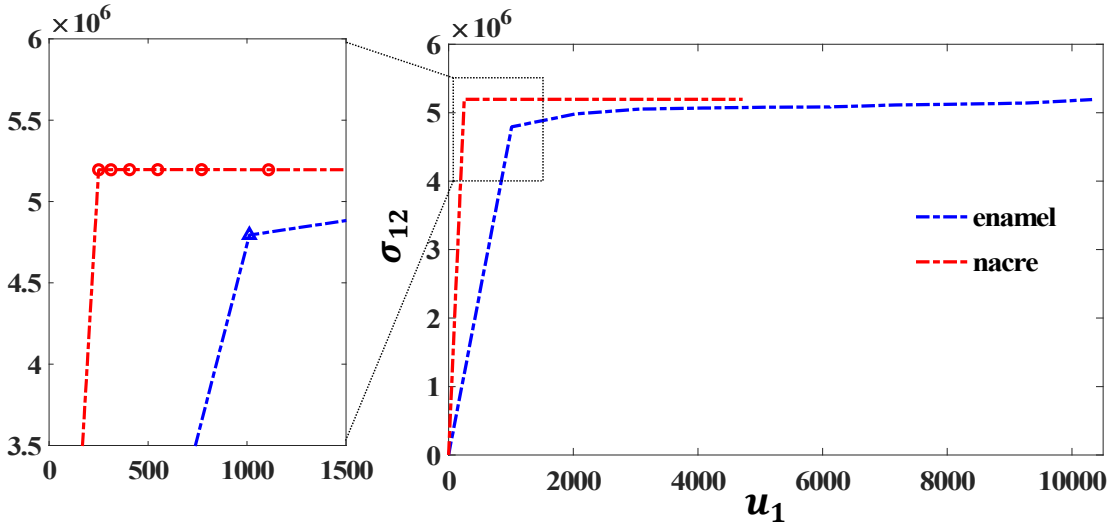

Fig. 12 The nacre and enamel structured composites' 1-directional shear stress-displacement diagram.

From Figure 12 one discerns that the nacre matrix experience higher shear stress value with the ongoing displacements, which indicate that under 1-directional loading, the nacre structure is more likely to experience the local fracture. Hence, from the fracture resistance perspective, the enamel structure is preferred under 1-directional loading.

Also, Figure 13 presents the shear stress-displacement of the 2-directional loading of enamel and nacre, respectively.

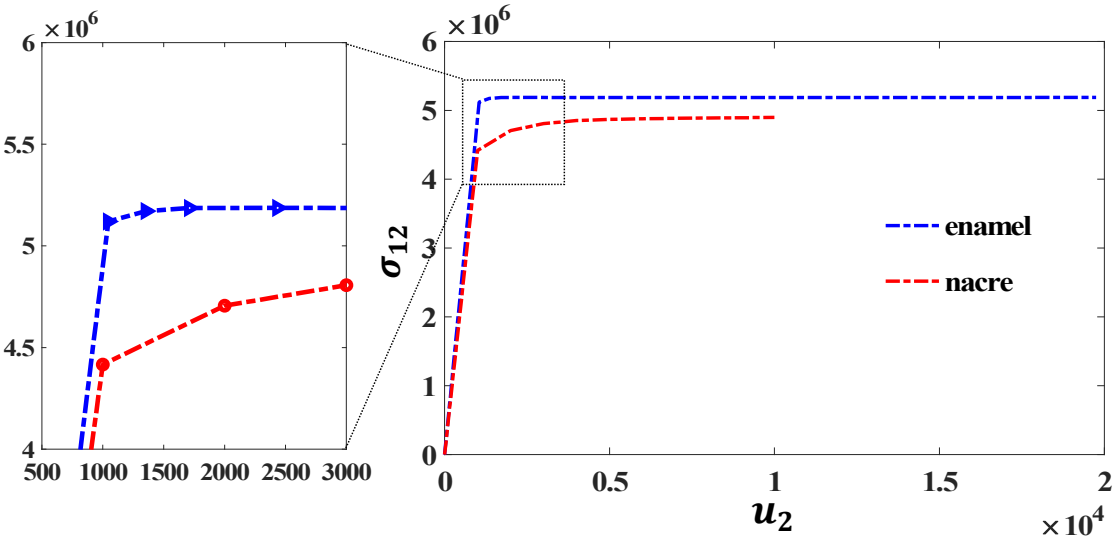

Fig. 13 The nacre and enamel structured composites' 2-directional shear stress-displacement diagram.

Following a similar thought trace, as presented in Figure 13 a higher stress value occurs on enamel under 2-directional loading, indicating a higher possibility for local fracture on enamel under such loads. Thenceforth, a nacre structure is preferred preventing local failure.

Optimization

Based on the previous discussions, we can adopt a basic guideline for designing a new structure exhibits high stiffness in both 1 and 2-directions, and high fracture resi-

-stance (low shear stress values on soft matrix) in both 1 and 2-directions: adopting the advantages of the structural displacement of both nacre and enamel in each direction. Hence, a new structural designation is presented as shown in Figure 14. The modelling of the structure carried out for simulations is shown in Figure 15.

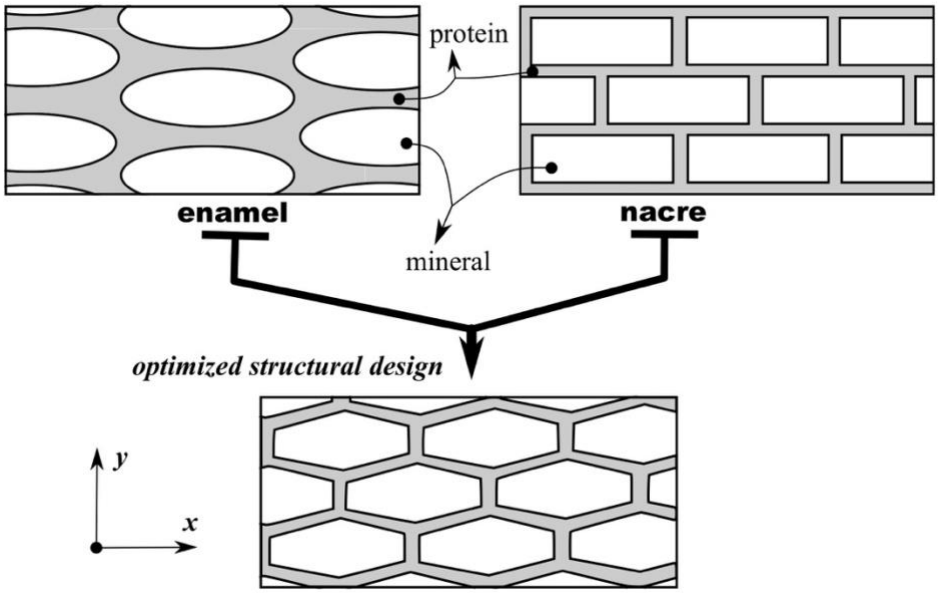

Fig. 14 Optimization process of the structural design based on the enamel and nacre microstructure.

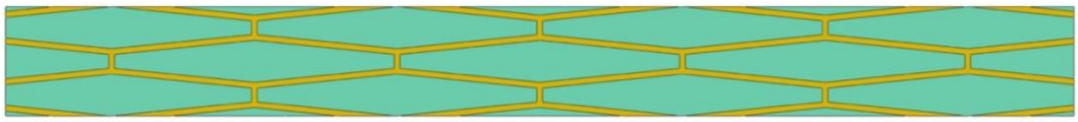

Fig. 15 Modelling of the optimized structure.

As the modeling presented, a verification for such an optimized structure's mechanical properties needed to be tested with simulations. We adopt the same thought trace as presented in the preceding part to calculate the 1 and 2-directional elastic moduli and its matrix shear stress-displacement curve with comparison to the nacre and enamel model, respectively.

The von Mises stress, 1-directional stress, and 1-directional strain distribution of the optimized structure undergoing 1-directional loading are shown as in Figure 16.

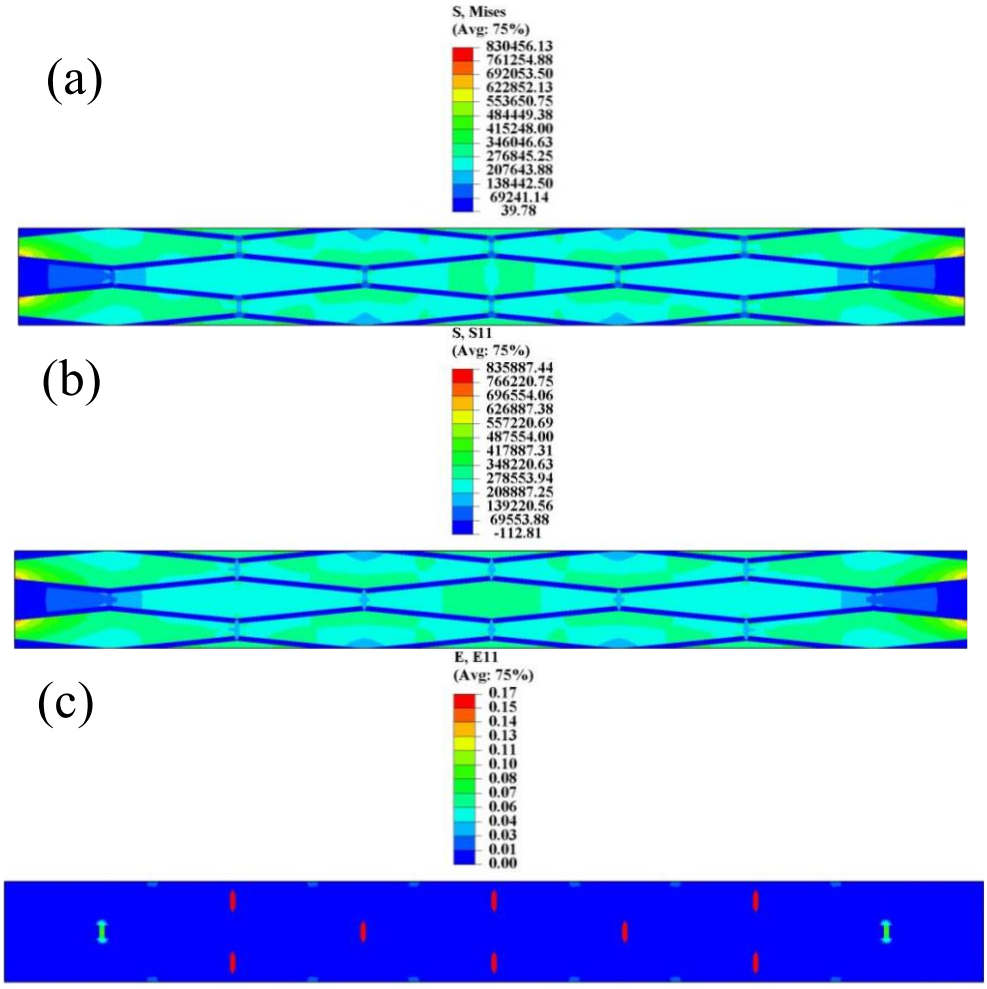

Fig. 16 The optimized structure's 1-directional mechanical distribution carried out for uniaxial tensile loading. (a) shear stress distribution. (b) 1-directional displacement distribution.

As presented in Figure 16, the 1-directional stress is the dominating stress as comparing Figure 16(a) with Figure 16(b). Generally, the 2-directional stress makes little effect on the total stress distribution. Furthermore, a local 1-directional strain concentration occurs while loading, howbeit the extended outline of the inclusions' shape could prevent longitudinal failure,

The von Mises stress, 2-directional stress, and 2-directional strain distribution of the optimized structure undergoing 2-directional tensile loading are shown as in Figure 17.

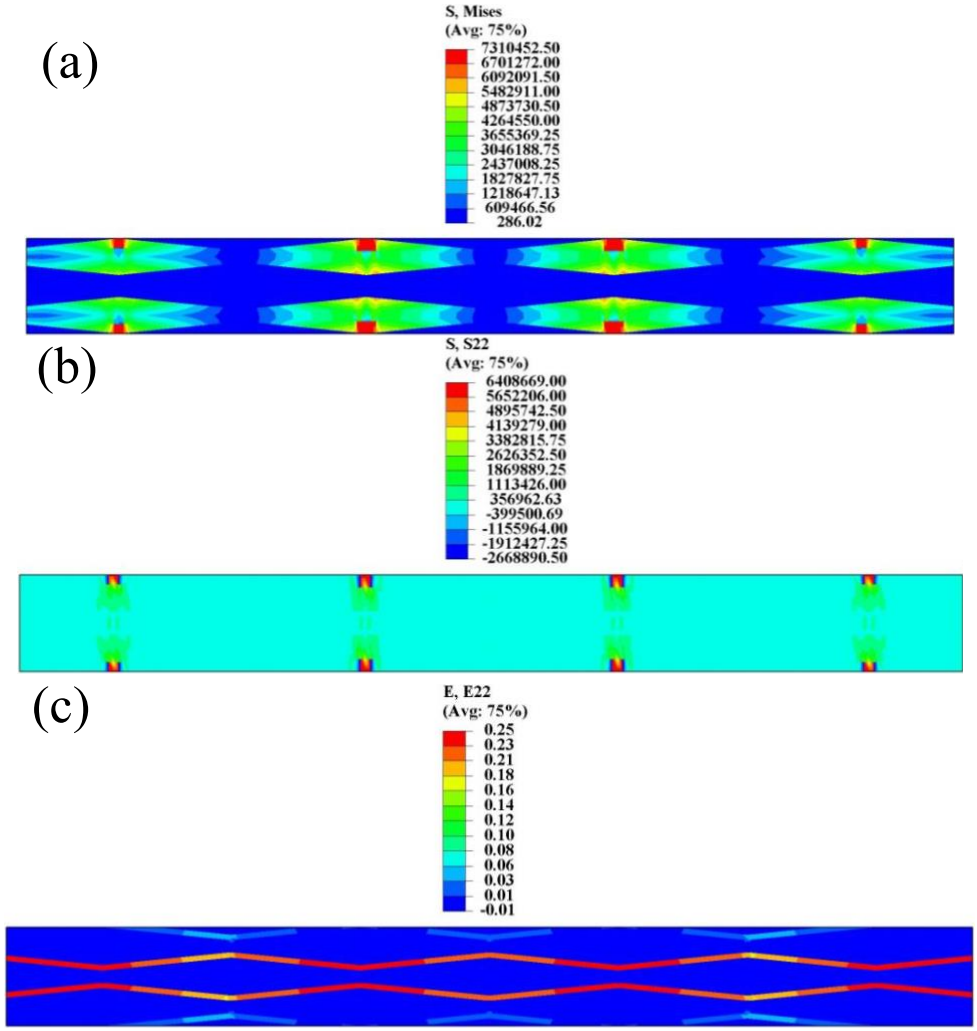

Fig. 17 The optimized structure's 2-directional mechanical distribution carried out for uniaxial tensile loading. (a) shear stress distribution. (b) 1-directional displacement distribution.

Similarly, one observes the 2-directional stress is not the main stress dominating the stress distribution of the whole structure comparing Figure 17(a) with Figure 17(b). Moreover, strain concentration along 1-directional edges occurs, indicating a possible form of the materials' failure.

Following previous steps, we calculate the elastic moduli for the optimized model in 1 and 2-directions and compare such results with the stiffness of the nacre and enamel model. The results are shown in Table 2 and as illustrated in Figure 18.

Structure	enamel	nacre	optimized structure	
1-directional Stiffness	10611974.6923077	79478880.8205128	85044895.0769231	[Pa]
2-directional Stiffness	7946666.13612566	2603749.64921466	9657233.08900524	

Tab. 2 The 1 and 2-directional stiffness calculation results of enamel, nacre, optimized structure, respectively.

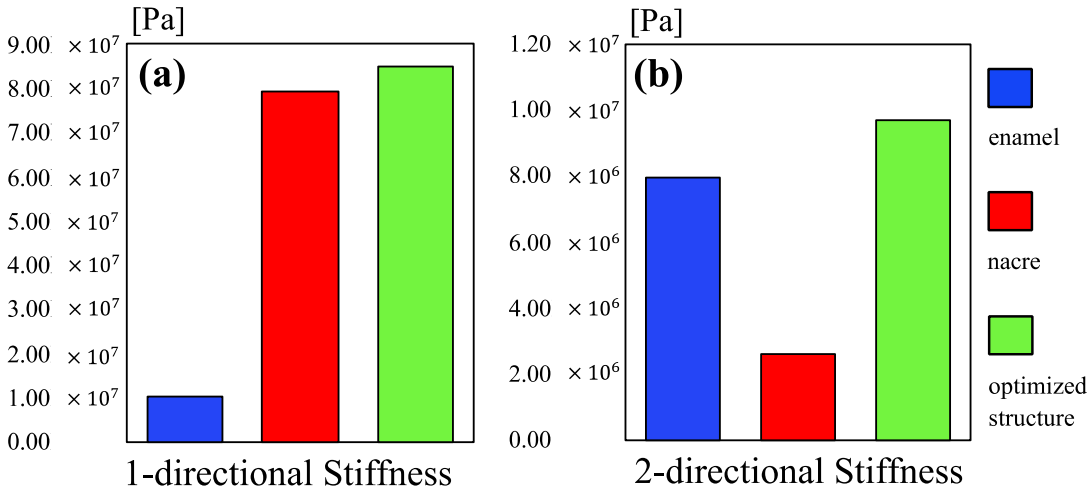

Fig. 18 The comparison of the structure's stiffness. (a) the 1-directional stiffness of nacre, enamel, and optimized model, respectively. (b) the 2-directional stiffness of nacre, enamel, and optimized model, respectively.

From the calculation results, one discerns that the optimized model robustly increases the stiffness in both 1 and 2-directions, respectively. Such increases, as mentioned, could be explained by the adoption of the characteristics of both nacre and enamel in both directions.

Subsequently, the possibility of local failure is hence be estimated by analyzing the shear stress distribution. As discussed previously, a perfectly plastic material model is adopted for the description of the soft matrix in the optimized model.

Figure 19 presents the shear stress distribution of the optimized model's matrix and the 1-directional displacement distribution when a 1-direction loading is applied.

Figure 20 presents the shear stress distribution of optimized model's matrix and the 2-directional displacement distribution when a 2-direction loading is applied.

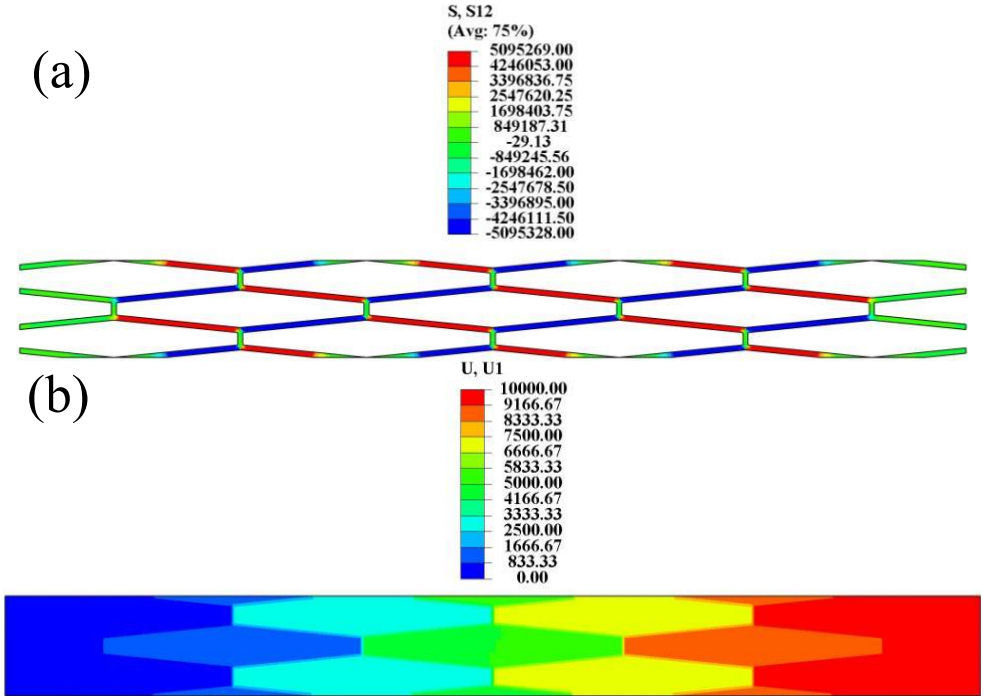

Fig. 19 The optimized structure's 1-directional mechanical distribution carried out for uniaxial tensile loading. (a) shear stress distribution. (b) 1-directional displacement distribution.

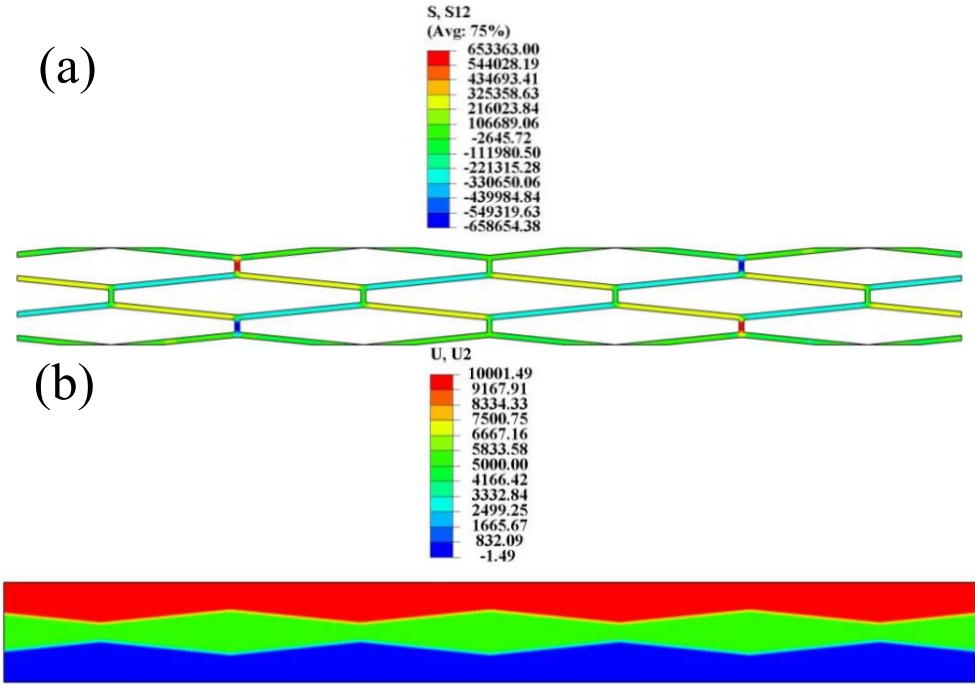

Fig. 20 The optimized structure's 2-directional mechanical distribution carried out for uniaxial tensile loading. (a) shear stress distribution. (b) 2-directional displacement distribution.

For both Figure 19(a) and Figure 20(a) indicate a high shear stress concentration along the loading direction. Such high shear stress concentration might indicate the fracture pattern of the optimized model. Also, from what is shown in Figure 20(b), with Figure 17(c) indicating a deformation pattern in 2-directional loading.

Based on the calculation results, a shear stress-displacement curve is given in each direction as shown in Figure 21.

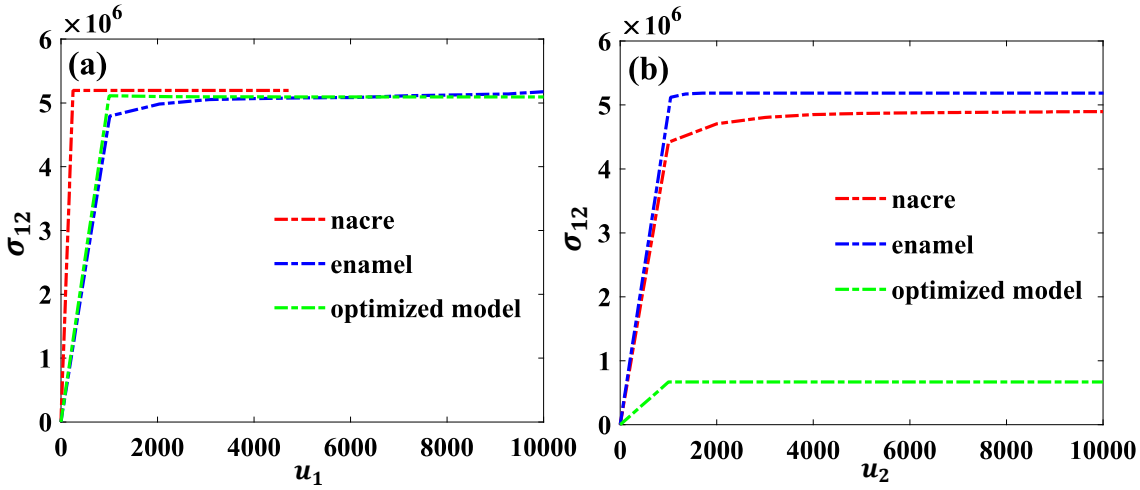

Fig. 21 The shear stress-displacement relationship. (a) the 1-directional curve of nacre, enamel, and optimized model, respectively. (b) the 2-directional curve of nacre, enamel, and optimized model, respectively.

Based on Figure 21(a), one can observe that the optimized model's shear stress is generally the same value as the enamel structure. Notwithstanding, the shear stress is greatly reduced pertaining to displacement under 2-directional loading for the optimized model comparing with nacre and enamel as shown in Figure 21(b). Such results indicate that the structural design is generally successful with regard to preventing the local failure, especially in the 2-directional as the shear stress value is greatly reduced from Figure 21(b). even the shear stress value is not greatly reduced, a generally similar value with the enamel also validates the design.

Conclusion

Biomaterials such as nacre and enamel display superior mechanical properties including high stiffness, high toughness, and fracture resistance. Such properties are employed through a specific hierarchical architecture composite, usually including a hard inclusion and soft matrix. Nacre and enamel both display such structure (Figure 1, Figure 2). To study such structures, we carry out simulations employ a perfect plasticity model for the soft matrix (Table 1), usually consist of protein. In the study, we test the 1 and 2-directional elastic moduli for nacre and enamel, respectively (Equation 1-Equation 3). We also estimate the composites' fracture resistance through analyzing the soft matrix's shear stress, in which we employ a criterion that the material fails when the matrix shear stress reaches a critical value.

For the calculation of the elastic moduli of the two materials, a directional tensile loading is carried out and the Mises stress, directional stress, and strain are illustrated for enamel (Figure 3, Figure 4) and nacre (Figure 5, Figure 6). The calculation results show that the nacre structure exhibits higher stiffness in 1-direction and enamel exhibits higher stiffness in 2-direction (Figure 7). Also, based on the given criterion, under the tensile loading in the two directions, the shear stress of the soft matrix and the displacements of the whole composite's material is presented for enamel (Figure 8, Figure 9) and nacre (Figure 10, Figure 11). Based on such results, the shear stress-displacement curve of the two composites in 1-direction (Figure 12) and 2-direction (Figure 13) is given respectively. Such results show that local fracture is more likely to occur on nacre in 1-direction and on enamel in 2-direction.

The obtained results indicate that both the enamel and nacre both displays some superior properties in specified conditions, compared with the other. Thenceforth, a basic thought trace is established: we need to employ both the characteristics of the two composites in the two directions to create an optimized structure that displays superior mechanical behavior. Hence, an optimized model is presented (Figure 14) and modeled (Figure 15).

To investigate and verify the mechanical properties, we also carry out tensile loading in the two directions and present the Mises stresses, 1 and 2-directional stresses, 1 and 2-directional strains for the optimized model (Figure 16, Figure 17). Calculation results contend the optimized structure displays higher stiffness in both the directions than enamel and nacre (Table 2, Figure 18), which validate the design of the structure. For what is more, to test its fracture resistance, we also calculate the optimized structure's soft matrix 1 and 2-directional shear stress and displacement distribution (Figure 19, Figure 20). Similarly, a shear stress-displacement diagram is given indicating that the optimized structure displays the same level of fracture resistance as enamel in the 1-direction (Figure 21(a)). Notwithstanding, such a structure greatly reduces the shear stress value in 2-direction, indicating less chance to fail to occur on the composites. The optimized design could provide decent insights and guidelines for future manufacturing and composites' structural design.

Acknowledgement

The author would like to thank B. An for the valuable discussion.

References

[1] B. An. Constitutive modeling the plastic deformation of bone-like materials. International Journal of Solids and Structures 92–93 (2016) 1–8

[2] B. An, Y. Liu, D. Arola, D. Zhang. Fracture toughening mechanism of cortical bone: an experimental and numerical approach. J. Mech. Behav. Biomed. Mater., 4 (2011), pp. 983-992

[3] An B., Zhang D. Bioinspired toughening mechanism: lesson from dentin. Bioinspir. Biomim., 10 (2015), Article 046010

[4] B. An, H. D. Wagner. Role of microstructure on fracture of dentin. Journal of the Mechanical Behavior of Biomedical Materials. Vol 59 (2016): 527-537. ISSN 1751-6161.

[5] M. Mirkhalafa, A. Sunesarab, B. Ashrafib, F. Barthelata. Toughness by segmentation: Fabrication, testing and micromechanics of architectured ceramic panels for impact applications. International Journal of Solids and Structures 158 (2019) 52–65

[6] Godaa M. Assidib S. Belouettarb J.F. Ganghoffera. A micropolar anisotropic constitutive model of cancellous bone from discrete homogenization. J. Mech. Behav. Biomed. Mater., 2012; Vol 16: 87-108

[7] Zhang Z., Zhang Y., Gao H. On optimal hierarchy of load-bearing biological materials. Proc. R. Soc. B, 278 (2011), pp. 519-525

[8] Su Y, Wang L, Wu X, Yi C, Yang M, Yan D, Cheng K, Cheng X. The spatial differences in bone mineral density and hip structure between low-energy femoral neck and trochanteric fractures in elderly Chinese using quantitative computed tomography. Bone, Vol 12

[9] B. Wang, X. Hub, P. Lua. Modelling and testing of large-scale masonry elements under three- T point bending – Tough and strong nacre-like structure enlarged by a factor of 20,000. Engineering Fracture Mechanics 229 (2020) 106961

[10] Horacio, Decanini & Juster, Allison & Latourte, Félix & Loh, Owen & Grégoire, David & Zavattieri, Pablo. (2011). Tablet-level origin of toughening in abalone shells and translation to synthetic composite materials. Nature communications. 2. 173. 10.1038/n

[11] F Barthelat. Nacre from mollusk shells: a model for high-performance structural materials. Bioinsp. Biomim. 5 (2010) 035001 (8pp)

[12] A. Ghazlana, T. Ngoa, T. Lea, T. Nguyena, A. Remennikov. Blast performance of a bio-mimetic panel based on the structure of nacre – A numerical study. Composite Structures 234 (2020) 111691.

[13] A. Shi, Y. Li, W. Liu, J. Xu, D. Yan, J. Lei, Z. Li. Highly thermally conductive and mechanically robust composite of linear ultrahigh molecular weight polyethylene and boron nitride via constructing nacre-like structure. Composites Science and Technology

[14] D. Bajaj, D. Arola. Role of prism decussation on fatigue crack growth and fracture of human enamel. Acta Biomaterialia 5 (2009) 3045–3056.

[15] M. Yahyazadehfar, D. Bajaj, D. Arola. Hidden contributions of the enamel rods on the fracture resistance of human teeth. Acta Biomaterialia 9 (2013) 4806–4814

[16] M. Yahyazadehfar, D. Arola. The role of organic proteins on the crack growth resistance of human enamel. Acta Biomaterialia 19 (2015) 33–45.

[17] N. Zhang, X. Wang, W. Xiang, Y. Zhong, F. Yana, B. Jiang. Hierarchy structure and fracture mechanisms of the wild wolf tusk's enamel. Materials Science & Engineering C 106 (2020) 110277.

[18] J. Koldehoff, M. V. Swain, G. A. Schneider. The geometrical structure of interfaces in dental enamel: A FIB-STEM investigation. Acta Biomaterialia 104 (2020) 17–27.